UNIVERSITY OF
GLOUCESTERSHIRE

This is a peer-reviewed, final published version of the following document and is licensed under Creative Commons: Attribution 4.0 license:

Simms, Alexander R, Best, Louise ORCID logoORCID: https://orcid.org/0000-0003-3731-054X, Shennan, Ian, Bradley, Sarah L, Small, David, Bustamante, Emmanuel, Lightowler, Amy, Osleger, Dillon and Sefton, Juliet (2022) Investigating the roles of relative sea-level change and glacio-isostatic adjustment on the retreat of a marine based ice stream in NW Scotland. Quaternary Science Reviews, 277. Art 107366. doi:10.1016/j.quascirev.2021.107366

Official URL: http://dx.doi.org/10.1016/j.quascirev.2021.107366
DOI: http://dx.doi.org/10.1016/j.quascirev.2021.107366
EPrint URI: https://eprints.glos.ac.uk/id/eprint/10593

Disclaimer

The University of Gloucestershire has obtained warranties from all depositors as to their title in the material deposited and as to their right to deposit such material.

The University of Gloucestershire makes no representation or warranties of commercial utility, title, or fitness for a particular purpose or any other warranty, express or implied in respect of any material deposited.

The University of Gloucestershire makes no representation that the use of the materials will not infringe any patent, copyright, trademark or other property or proprietary rights.

The University of Gloucestershire accepts no liability for any infringement of intellectual property rights in any material deposited but will remove such material from public view pending investigation in the event of an allegation of any such infringement.

PLEASE SCROLL DOWN FOR TEXT.

Quaternary Science Reviews 277 (2022) 107366

Contents lists available at ScienceDirect

Quaternary Science Reviews

journal homepage: www.elsevier.com/locate/quascirev

Investigating the roles of relative sea-level change and glacio-isostatic adjustment on the retreat of a marine based ice stream in NW Scotland

Alexander R. Simms [a, *], Louise Best [b], Ian Shennan [c], Sarah L. Bradley [d], David Small [c], Emmanuel Bustamante [c], Amy Lightowler [c], Dillon Osleger [a], Juliet Sefton [c]

[a] Department of Earth Science, University of California Santa Barbara, USA
[b] School of Natural and Social Sciences, University of Gloucestershire, UK
[c] Department of Geography, Durham University, UK
[d] Department of Geography, The University of Sheffield, UK

ARTICLE INFO

Article history:
Received 6 October 2021
Received in revised form
28 December 2021
Accepted 29 December 2021
Available online xxx

Handling Editor: A. Voelker

ABSTRACT

The record of ice-sheet demise since the last glacial maximum (LGM) provides an opportunity to test the relative importance of instability mechanisms, including relative sea-level (RSL) change, controlling ice-sheet retreat. Here we examine the record of RSL changes accompanying the retreat of the Minch Ice Stream (MnIS) of northwest Scotland during the deglaciation following the LGM as well as use the record to provide additional age constraints on a local late-glacial readvance known as the Wester Ross Readvance. We use new and existing records of RSL change obtained from isolation basins in Wester Ross along the flanks of the former MnIS to test available glacial-isostatic adjustment (GIA) predictions of the deglacial RSL history for the region. Using these GIA model predictions we examine the nature of RSL change across the retreating front of the MnIS through the early deglaciation. Our new radiocarbon ages from these basins confirm the timing of deglaciation within the inner trough of the former MnIS as well as refines the age of the Wester Ross Readvance, both established by earlier cosmogenic-based studies. We find that the Wester Ross Readvance culminated around 15.8 ± 0.1 ka, slightly earlier than recent suggestions. Near Gairloch, Wester Ross, RSL fell from a marine limit ~20 m above present at ~16.1–16.5 ka. Three isolation basins record RSL fall over the following ~0.8 ka allowing a comparison between GIA predictions and RSL observations. Our new analyses suggest that the rate of RSL rise increased at the ice front, in concert with the MnIS encountering a landward sloping bed potentially aiding the rapid retreat of the MnIS from 17.6 to 16.4 ka BP. This observation suggests that GIA during deglaciation does not necessarily induce a stabilizing RSL change to marine-based ice streams as some models have suggested. Along indented ice margins, the RSL field at the front of individual ice streams may be governed by the regional GIA signal driven by the ice sheet as a whole, rather than the local ice front. In addition, the stabilizing impact of post-glacial rebound is dependent on an Earth rheology weak enough to respond quickly to the ice-sheet retreat. In the case of the MnIS, the RSL experienced at the front of the ice stream was likely governed by the earlier ice mass extent, the larger ice masses lying to the east and south of the highly indented ice front, and the relatively strong Earth rheology beneath the British Isles. Thus, the geometry of the ice sheet margins, such as those in Greenland and Antarctica today, and the Earth rheology beneath them need to be taken into account when considering the stabilizing impact of post-glacial rebound on marine ice sheet retreat.

© 2022 The Authors. Published by Elsevier Ltd. This is an open access article under the CC BY license (http://creativecommons.org/licenses/by/4.0/).

1. Introduction

Rapid ice-sheet retreat provides a mechanism for large increases in the rate of sea-level rise (Mercer, 1978). One common mechanism for rapid retreat is the collapse of ice streams (Dowdeswell

* Corresponding author.
E-mail address: asimms@geol.ucsb.edu (A.R. Simms).

https://doi.org/10.1016/j.quascirev.2021.107366
0277-3791/© 2022 The Authors. Published by Elsevier Ltd. This is an open access article under the CC BY license (http://creativecommons.org/licenses/by/4.0/).

et al., 2008). Understanding the controls on ice-stream collapse may thus provide clues about potential warning signs within the existing ice sheets and their fate with respect to ongoing warming. Numerical models used to predict the behavior of ice sheets and ice streams during retreat point to differences in their rates of retreat based on both internal and external drivers including relative sea-level (RSL) rise and glacial isostatic adjustment (GIA) feedbacks (e.g. Weertman, 1974; Gomez et al., 2010; Gandy et al., 2018; Kachuck et al., 2020). However, like any numerical model, their real test relies on observations of ice-sheet behavior at the temporal and spatial scales of extant ice sheets. One way to perform such a test is to compare model predictions to empirical reconstructions of the past behavior of ice sheets (e.g. Gandy et al., 2018; Bradwell et al., 2019).

Ice streams were common features developed along the margins of the Last Glacial Maximum (LGM) ice sheets (e.g. Bradwell et al., 2019; Bart and Tulaczyk, 2020; Greenwood et al., 2021). Recent efforts (e.g. BRITICE-CHRONO project; Clark et al., 2017) to better define the history of the British-Irish Ice Sheet (BIIS) have documented the rapid retreat of many of the former ice streams draining its margin (Bradwell et al., 2008b, 2019; Small et al., 2018; Davies et al., 2019; Scourse et al., 2019). One of these large ice streams – the Minch Ice Stream (MnIS; Bradwell and Stoker, 2015; Bradwell et al., 2019) – underwent a prolonged retreat, punctuated by a period of accelerated retreat (>60 m/yr) around 17.9–15.0 ka between the Outer Hebrides and the mainland of northwest Scotland (Fig. 1). The nature of the retreat appears to be largely governed by the geomorphology of its trough, where the timing and

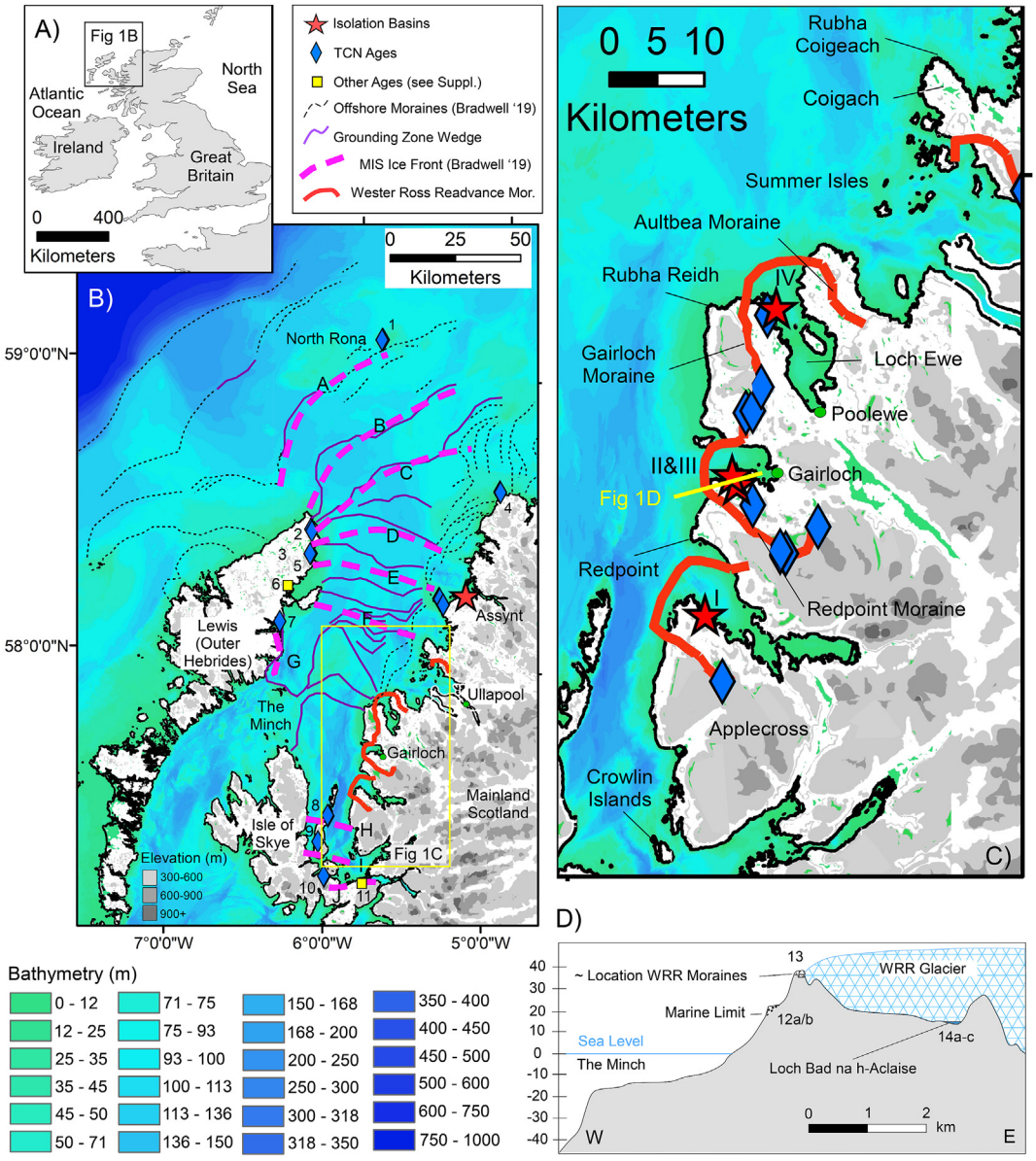

Fig. 1. (A) Sequence of events used in our OxCal modeling alongside (B–C) maps showing the location of the Minch Ice Stream (MnIS) front (dashed purple line) through time and (D) the locations of our new and existing RSL (red stars) and TCN (blue diamonds; Bradwell et al., 2019; Ballantyne and Stone, 2012) data as well as the Wester Ross Readvance moraines (solid orange line; Robinson and Ballantyne, 1979) and other locations discussed in the text. (E) Topographic profile through the Gairloch Peninsula showing the spatial relationship between the shorelines marking the marine limits of Wester Ross, the Wester Ross Readvance moraines, and the isolation basins used in our RSL reconstructions. Letters refer to the approximate locations of the MnIS through time (from Bradwell et al., 2019) while roman numerals refer to the RSL locations. I = Fearnbeg, II = Glac Bhuidhe, III = Loch Bad na h-Achlaise, and IV = Glac a' Chaochain (see the See Fig. S3 for more details as to their locations). Arabic numbers refer to the locations of the TCN and other ages used in the OxCal Model (Fig. S1). (For interpretation of the references to color in this figure legend, the reader is referred to the Web version of this article.)

location of rapid demise corresponds to its retreat into a bedrock-dominated region of reverse gradient (Gandy et al., 2018; Bradwell et al., 2019). Bradwell et al. (2019) pointed out that the MnIS underwent changes in retreat style independent of pronounced external perturbations (e.g. known climate events or global meltwater pulses). However, they did not examine what role GIA-driven RSL change may have played in the retreat history of the ice stream; a particularly difficult problem to address given the heterogeneous nature of RSL histories within the near-field region of the former BIIS (Shennan et al., 2018).

In this study we produce a new record of RSL change along the margins of the MnIS during its period of rapid retreat. We compare this new record, in addition to previously published records, to existing records of deglaciation and competing GIA model predictions of RSL change along the margins of the MnIS. Then, we use these GIA models to examine the record of RSL changes at the MnIS ice front during its retreat to determine what role RSL may have played in the ice stream's retreat.

2. Background

2.1. Last glacial maximum deglacial history and configuration of the NW BIIS

During the LGM, the BIIS merged with the Fennoscandian Ice Sheet to the east, covering the North Sea. To the west the BIIS extended to the shelf edge along its western and northern margins (Bradwell et al., 2008b, 2021; Hughes et al., 2016; Ballantyne and Small, 2018). During this maximum extent and through most of the early deglacial period the margins of the combined ice sheets were host to large ice streams (Bradwell et al., 2008b; Ballantyne and Small, 2018, Fig. 1). One of these ice streams flowed through what today is the Minch, the channel between the Outer Hebrides and the mainland of Western Scotland (Fig. 1).

At its maximum extent, the MnIS extended north over 260 km from the Isle of Skye to the shelf edge west of the modern island of North Rona (Stoker et al., 2009; Bradwell and Stoker, 2015; Bradwell et al., 2019) (Fig. 1). Its detailed retreat history was documented by a combined marine and terrestrial campaign of mapping its subglacial features and dating its retreat history (Bradwell et al., 2019). Sustained retreat of the MnIS commenced around 30 ka and continued to about 18.5 ka at which time its western fork experienced two periods of frontal collapse from 18.5 ka to 16.9 ka and a more pronounced retreat from 16.9 ka to 15.9 ka when the ice front encountered a bedrock dominated landward sloping seafloor (Gandy et al., 2018; Bradwell et al., 2019). This latter collapse was marked by a seven fold increase in retreat rates. Bradwell et al. (2019) concluded that the ice retreat behavior was governed more by the geometry and substrate of the trough than external forcing mechanisms such as climate events or meltwater pulses. They noted that the collapse of the ice stream coincided with the ice front retreating into a region with a retrograde bed and from a soft deformable substrate to a hard substrate. In addition, the ice stream encountered a bifurcation in the trough itself and may have pinned on a bedrock high at the junction point prior to its rapid retreat. However, they were unable to determine the role of RSL in MnIS retreat.

2.2. Wester Ross Readvance

The Wester Ross Readvance (WRR) is recorded by a series of moraines on the eastern shore of the Minch in northwestern Scotland and was initially thought to record a pre- Loch Lomond (Younger Dryas; 12.9–11.7 ka), post LGM, advance of the western Scottish mainland glaciers (Robinson and Ballantyne, 1979; Sissons and Dawson, 1981). Moraines assigned to this readvance span >60 km from the Coigach in the north to Applecross in the south (Fig. 1). The first cosmogenic ages from WRR moraines ranged from 23.1 ± 4.0 ka to 11.0 ± 3.0 ka with a mean age of 16.3 ± 1.6 ka (Everest et al., 2006). Based on these ages, Everest et al. (2006) argued for a Heinrich event 1 (H1) climate driver for the WRR. Subsequent dating (Bradwell et al., 2008a; Ballantyne et al., 2009) revised the timing of the WRR to between 13.5 ± 1.2 ka to 14.0 ± 1.7 ka suggesting that the WRR represented a period of rapid short-lived cooling during the Older Dryas (13.9–14.1 ka). The most recent compilations of the Quaternary history of Scotland updated these ages using a revised production rate to place the age of the WRR at around 15.2 ka but with notably large error bars (Ballantyne and Small, 2018; Bradwell et al., 2019). Further independent dating evidence related to the timing of the WRR is critical to improve understanding of its potential climatic significance.

2.3. Scottish sea levels

Scotland, Great Britain and Ireland experienced a diverse range of RSL histories through the Late Pleistocene and into the Holocene (e.g. Shennan et al., 2018) due in part to the presence of the BIIS as well as the early deglacial persistence of ice caps (Small and Fabel., 2016; MacLeod et al., 2011; Palmer et al., 2020). Over NW Scotland, RSL generally fell from a few 10's of meters above present during the Late Pleistocene to below present sea level in the early Holocene (~8–11.7 ka; Selby and Smith, 2007; Hamilton et al., 2015; Smith et al., 2019; Shennan et al., 2000, 2018; Best et al., in press). This lowstand was followed by a rise in sea levels to 5–7 m above present during the mid-Holocene (~6–7 ka). Since the mid-Holocene, sea levels have steadily fallen (Hamilton et al., 2015; Shennan et al., 2018). The details of the Late Pleistocene fall in RSL across western Scotland including its magnitude and rate are still a work in progress as is the ability of current GIA models to replicate these RSL observations (Shennan et al., 2018). One difficulty in working out the RSL history of western Scotland is the inability of most GIA models to correctly match observations for both eastern and western Scotland. The models of Bradley et al. (2011) appear to fit the sea-level observations of eastern Scotland but fail to produce RSLs high enough to match the marine limits and other RSL indicators of western Scotland (Bradley et al., 2011; Shennan et al., 2018). Similarly, the models of Kuchar et al. (2012) match the available RSL constraints from portions of western Scotland but are generally regarded as too thick and produce RSL predictions that are too high for eastern Scotland (Shennan et al., 2018).

2.4. Study areas

We provide new data from three bogs and shallow lake basins across NW Scotland: two isolation basins approximately 5 km southwest of Gairloch, and a third basin approximately 10 km north of Poolewe (Fig. 1; Table S1). The coastal regions of NW Scotland are marked by low-relief (<125 m) glacially-carved hills and depressions: cnoc and lochan terrain. Several small lakes fill some of these depressions including Loch Bad na h-Achlaise, while other depressions are filled with peat-bogs such as Glac Bhuidhe and Glac a' Chaochain. All three lie within the moraine limits of the WRR (Robinson and Ballantyne, 1979) (Fig. 1).

Loch Bad na h-Achlaise is a small lake (~0.2 km^2) lying at an elevation of ~13.5 m above sea level. It is connected to the ocean by a 500 m long east-flowing outlet stream that runs into a small cove within Loch Gairloch (Fig. S1). Glac Bhuidhe is an ~1 km long N–S oriented valley that runs from the larger valley filled with Loch Bad na h-Achlaise to Loch Gairloch. Glac Bhuidhe has an internal drainage divide located ~150 m north of Loch Bad na h-Achlaise.

The peat bog sampled lies immediately beneath a step in the topography north of the drainage divide at an elevation of ~19.5 m (Fig. S1). Glac a Chaochain lies at an elevation of ~8 m within a shallow valley ending in the ocean at the confluence of Loch Ewe and the Minch (Fig. 1).

3. Methods

3.1. Sediment cores and RSL reconstruction

Fourteen Russian cores were collected along the southern shore of Loch Bad na h-Achlaise (Fig. S1). These cores were photographed and described in the field. The most complete and longest core (LBA18-11R) was taken back to the laboratory for analysis at Durham University. An additional 13 gouge cores were taken near the outlet stream of Loch Bad na h-Achlaise to survey the elevation of the sill separating it from the ocean. Thirty two gouge cores were collected within Glac Bhuidhe to define the shape of the basin and elevation of the sill. These 32 cores guided the collection of 10 additional Russian cores used to map the stratigraphy within the basin. The Russian cores were photographed and described in the field and the longest and most complete core (GB17-3) was kept for laboratory analysis at Durham University. We also obtained another core from a third basin, Glac a' Chaochain (IAN19-07), whose stratigraphy was similar to that of the other basins. However, the core showed signs of deformation within the lacustrine portions of the core and its sill height was not adequately determined, thus ages from it were only used to establish a minimum time of deglaciation of the region.

Samples were prepared for diatom and foraminifera analysis following standard procedures (e.g. Shennan et al., 2000). Magnetic susceptibility (MS) was collected at 2 mm spacing for the lower ~4 m of core LBA18-11R and ~2 m of core GB17-3 using a Geotek Multi Sensor Core Logger (MSCL − S). All cores and sill heights were surveyed with a Leica 1200 differential GPS and Leica Automatic Optical Level in reference to Ordnance Survey benchmarks, giving elevations to Ordnance Datum Newlyn (m OD). We estimate the indicative meanings of dated samples from the biostratigraphy and use these to give RSL reconstructions as the basins became isolated from the sea (Table 1). For raised shorelines we assume their indicative meaning approximates mean high water springs (MHWS).

Seven samples from core LBA18-11, five samples from core GB17-3, and two samples from IAN19-07 were collected for radiocarbon analysis (Table 1). Material for dating was obtained by sieving approximately 0.5 cm^3 of core sediments with a 63 μm mesh and picking under a binocular microscope either large plant fragments (1–2 cm), individual *Charophyte oogonia* seeds (~1.0–0.5 mm), or masses of small plant fibers and fragments (length <1 cm; diameter <50 μm) isolated physically via flotation ("plant fibers" in Table 1). The organic material was graphitized and measured for ^{14}C concentrations via accelerated mass spectroscopy at the University of California Irvine Keck Carbon Cycle AMS Facility. Radiocarbon ages were calibrated using the OxCal 4.4 online program and the standard Northern Hemisphere atmospheric curve (Reimer et al., 2020).

3.2. Existing age constraints and MnIS retreat model

We recalibrated existing radiocarbon ages from previous studies of isolation basins near Fearnbeg on the Applecross Peninsula (Shennan et al., 2000) and the Assynt region (Hamilton et al., 2015) (Fig. 1). We also included a minimum deglacial age of 14.19–14.00 ka based on the presence of the Borropol Ash within Loch Ashik on the Isle of Skye (Brooks et al., 2012; Bronk Ramsey et al., 2015). Terrestrial cosmogenic-nuclide (TCN) ages from Bradwell et al. (2019) along the margins of the MnIS as well as those collected on WRR moraines (Bradwell et al., 2008a; Ballantyne et al., 2009) were recalculated using the v3 of the online calculator previously known as the CRONUS-Earth online exposure age calculator (Balco et al., 2008) using the nuclide-dependent scaling scheme of Lifton et al. (2014) and the local production rate of Fabel et al. (2012). Given the relatively large uncertainties associated with TCN ages *vis a vis* radiocarbon ages it is the latter that dominate the Bayesian age models, and thus our results and conclusions are not sensitive to the choice of production rate or scaling scheme.

Upon compilation of existing TCN and radiocarbon ages as well as our new radiocarbon ages, we explored a number of *prior* model setups within a Bayesian sequence model in OxCal 4.4 (Bronk Ramsey, 2009). We used the sequence of events within the MnIS as reported by Bradwell et al. (2019) as a starting point. We then added our new ages to the end of their sequence in addition to the recalculated TCN ages from the WRR moraines (Fig. S2). We assumed that the MnIS retreated to near the location of the Isle of Skye followed by the synchronous retreat of the ice within its tributaries along the eastern coast of the Minch. All the WRR TCN ages were considered a single "phase" (cf. Ballantyne and Small, 2018) within the Oxcal program followed by our new radiocarbon ages. Our other *prior* OxCal age model scenarios included a set of models in which the WRR TCN ages and our new ^{14}C ages were divided up geographically and only included the Bradwell et al. (2019) TCN ages outboard of those geographic areas.

In addition, we also added temporal constraints to the OxCal model based on the marine limits at Fearnbeg and Gairloch. Although these marine limits within Wester Ross have been surveyed by Sissons and Dawson (1981) and Dawson (2009), they have yet to be dated directly. We approximated the age of these features (Age_{ML}) by extrapolating the elevation (E_{SL}) of our RSL indicators to the elevation of the marine limits (E_{ML}) using the RSL rate of change ($Rate_{RSL}$) from the Kuchar et al. (2012) GIA model predictions at Loch Bad na h-Achlaise and Fearnbeg with the following equation:

$$Age_{ML} = Age_{SL} + (E_{ML} - E_{SL}) / Rate_{RSL} \quad (1)$$

Where Age_{SL} is the age of the RSL indicators. Although uncertainty remains in the GIA predictions for this portion of Scotland, the rates of change are very similar among the available GIA models during this time period with most of their differences occurring among their timing and maximum height rather than rates of RSL change. The uncertainty for this estimate was determined by using equation (1) on both the upper and lower error limits of Age_{SL}.

3.3. GIA predictions

In order to estimate RSL changes at the MnIS ice front, we considered three GIA models, Kuchar et al. (2012) (Kuchar model), Bradley et al., 2011 (B2011 model) and the new reconstruction from the BRITICE-CHRONO project (Clark et al., 2017; BC2020 model). The key difference in these three models is in the development of the input BIIS reconstructions. The Kuchar model incorporates the output from a dynamic ice sheet model (Hubbard et al., 2009); both the B2011 and BC2020 have ice sheet loading histories produced using geomorphological data, with the latter adopting the output from a simple plastic ice sheet model (Gowan et al., 2016) constrained to the larger landform dataset from the BRITICE-CHRONO project (i.e Bradwell et al., 2019; Clark et al., 2017). Each GIA model is combined with a specific optimum Earth model determined by

Table 1
New radiocarbon ages obtained for this study.

Source	Location	UCIAMS	Core, Depth (cm)	Material	14C age (BP)	Error (Yr)	Calendar Age[a]	Error	Error	Bayesian	Error	Error	Sill (m)	Error (m)	Indicative Meaning	Error (m)	RSL (m)	Error (m)
		#					Median (Yr)	Range (+)	Range (−)	Age (Yr)[b]	Range (+)	Range (−)						
This Study	Loch Bad na h-Achlaise	208,389	LBA18-11R, 233	Plant fibers	8385	25	9400	9490	9310	9400	9490	9310						
This Study	Loch Bad na h-Achlaise	208,390	LBA18-11R, 268	Plant fibers	9885	30	11,310	11,400	11,220	11,310	11,400	11,220						
This Study	Loch Bad na h-Achlaise	208,391	LBA18-11R, 310	Plant fibers	10,900	30	12,820	12,890	12,750	12,820	12,890	12,750						
This Study	Loch Bad na h-Achlaise	208,393	LBA18-11R, 337	Plant fibers	11,165	30	13,090	13,170	13,010	13,090	13,170	13,010						
This Study	Loch Bad na h-Achlaise	208,394	LBA18-11R, 400	Plant fibers	12,280	35	14,430	14,790	14,080	14,200	14,340	14,070						
This Study	Loch Bad na h-Achlaise	208,396	LBA18-11R, 530	Plant fibers	13,185	45	15,830	15,990	15,670	15,840	15,980	15,710	12.65	0.05	MHW - Spring	0.4	10.15	0.4
This Study	Loch Bad na h-Achlaise	208,397	LBA18-11R, 536	Plant fibers	13,240	50	15,900	16,080	15,720	15,880	16,020	15,750	12.65	0.05	MHW - Neap	0.4	11.35	0.4
This Study	Glac Buidhle	208,395	GB17-3, 489	Plant fibers	12,885	40	15,410	15,580	12,250									
This Study	Glac Buidhle	208,354	GB17-3, 491	C. oogonia seeds	13,040	35	15,620	15,780	15,470									
This Study	Glac Buidhle	208,353	GB17-3, 496	Plant Frag.	12,690	35	15,130	15,260	15,000									
This Study	Glac Buidhle	200,636	GB17-3, 498	C. oogonia seeds	12,975	35	15,500	15,670	15,340									
This Study	Glac Buidhle	200,637	GB17-3, 513	Plant Frag.	11,880	170	13,750	14,150	13,360				17.26	0.1	HAT	0.4	14.15	0.4
This Study	Glac a' Chaochain	230,394	IAN19-07, 514	Plant Frag.	12,130	40	13,960	14,110	13,810									
This Study	Glac a' Chaochain	230,395	IAN19-07, 530	Plant Frag.	12,750	35	15,210	15,330	15,080									
Shennan et al. (2000)	Fearnbeg	AA28102	FB93−1.1	Plant Frag.	11,980	80	13,830	14,060	13,610				5.7	0.19	MHW - Spring	0.4	4.47	0.4
Shennan et al. (2000)	Fearnbeg	AA28101	FB93−1.2	Plant Frag.	12,280	75	14,440	14,830	14,040				5.7	0.19	MTL	0.4	5.95	0.4
Hamilton et al. (2015)	Assynt	Beta-390,107	Loch Duart Marsh (2)	Organics	12,670	80	14,980	15,360	14,610				1.95	0.1	MHW - Spring	0.4	0.35	0.4
This Study	Gairloch Marine Limit									16,300[c]	16,500	16,100	22	0.1	MHW - Spring	0.5	19.5	0.5
This Study	Applecross Marine Limit									15,800[c]	16,000	15,600	29.6	0.1	MHW - Spring	0.5	27.2	0.5

MHW = Mean High Water.
MTL = Mean Tide Level.
HAT = Highest Astronomical Tide.
[a] OxCal 4.4 (Reimer et al., 2020).
[b] Depositional model (Bronk Ramsey, 2009)
[c] Age using Equation (1).

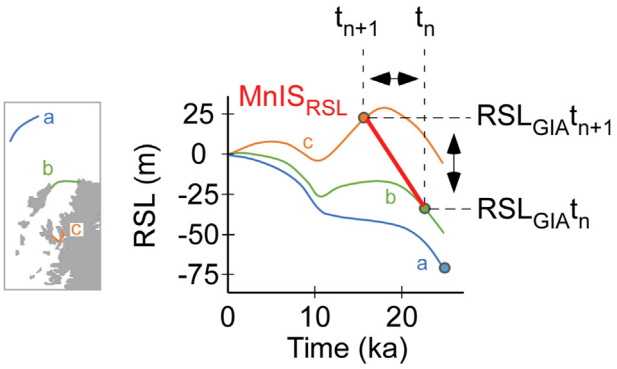

Fig. 2. Conceptual model showing how rates of sea-level by the Minch Ice Stream ice front were determined. Top row panels illustrate GIA predicted rates of RSL change from 27-10 ka at three locations of the Minch Ice Stream ice front, a, b, and c. The bottom row shows how RSL_{MnIS} is calculated from the GIA predictions at t_0, t_n, and t_{n+1}. See text for details.

comparisons to the British Isles sea-level database (Shennan et al., 2018).

Rates of RSL change experienced at the front of the MnIS ($MnIS_{RSL}$) were calculated in the following manner:

$$MnIS_{RSL} = (RSL_{GIA}t_n - RSL_{GIA}t_{n+1}) / t_n - t_{n+1} \quad (2)$$

Where $RSL_{GIA}t_n$ is the GIA-predicted RSL at the front of the MnIS at time t_n and $RSL_{GIA}t_{n+1}$ is the GIA-predicted RSL at the MnIS front at the next time step, t_{n+1} (Fig. 2; Table 2). We used a linear interpolation between time steps within the GIA model for our RSL calculations.

4. Results

4.1. Basin stratigraphy

4.1.1. Loch Bad na h-Achlaise, sill elevation: 12.65 ± 0.05 m OD

The cores obtained along the southwestern shore of Loch Bad na h-Achlaise contain pink silt at their bases, which in one core overlies bedrock (Figs. 3, 4, S3). This pink silt gradually transitions into a blue-grey laminated silt bed up to 65 cm thick (Figs. 3–5). This blue-grey silt bed contains occasional plant fragments, marine diatoms, as well as very fine sand (Fig. 5). The grey laminated silt gradationally transitions up core to green-brown laminated organic mud at 536 cm (Figs. 3–5). The laminations within the organic mud are generally composed of larger, often darker colored plant fragments. The organic mud is also interrupted by more sandy or silty laminations or beds. A prominent shift back to more grey silt is encountered at ~440 cm (Figs. 3–5). This shift is marked by a spike in MS (Fig. 5). Both the grey color and high MS gradationally shift back to the more organic-rich mud over several tens of centimeters. However, that gradual change is abruptly broken by a prominent thin bed of silty organic mud with a distinct red coloration at a depth of 403 cm (Fig. 3). The red silty organic mud bed attains a thickness of 2–3 cm and correlates to a peak in MS (Fig. 5). Another prominent bed of grey-colored silt is found above the organic mud bed overlying the "red silt" and attains a thickness of nearly 50 cm in cores LBA18-12 and LBA18-11 (Figs. 3, 4, S2). In at least one of the cores the upper contact of the upper grey-silt bed is inclined indicating erosion. Above the organic mud interbedded with silt is 2–3 m of herbaceous dark brown peat (Figs. 3 and S3).

4.1.2. Glac Bhuidhe, sill elevation: 17.26 ± 0.10 m OD

The basin fill within Glac Bhuidhe is composed of 3–6 m of late Pleistocene through Holocene sediments (Figs. 3 and S4). Similar to Loch Bad na h-Achlaise, it generally contains a basal unit of pink silt gradationally overlain by an ~50 cm thick bed of blue-grey weakly laminated silt (Figs. 3 and 5). This silt bed has 1–2 thin lamina of sandy silt and contains marine diatoms (Fig. 5). The upper-most of these sandy silt laminations may represent an erosional surface. The blue-grey silt is abruptly overlain by up to ~125 cm of well-laminated brown-green organic mud with a prominent ~10–20 cm bed of grey more silty organic mud with a few laminations of sand (Fig. 5). In core GB17-3, this upper grey silty bed also contains clay rip-up clasts. The organic mud is overlain by 2–3 m of herbaceous dark brown peat (Figs. 3 and S4).

4.2. Chronology

4.2.1. New ages

The seven radiocarbon ages obtained from core LBA18-11 from Loch Bad na h-Achlaise are in stratigraphic order (Figs. 4 and 5). The calibrated ages span from 15.90 cal ka BP (16.08–15.72 cal ka BP) at the contact between the marine and lacustrine units at a depth of

Table 2
OxCal age model results and comparison to the age assignments of Bradwell et al. (2019).

Location	Bradwell et al. (2019)			This study			Difference (ka)
	Mean (ka)	Uncer. (95%, ka)	Retreat Rate (m/yr)	Mean (ka)	Uncer. (95%, ka)	Retreat Rate (m/yr)	
A	27.1	1.0		27.2	1.5		0.1
B	24.8	1.0	10.0	25.2	1.6	11.4	0.4
C	23.3	0.7	11.3	24.2	1.2	16.0	0.8
D	22.2	0.7	19.2	22.9	1.1	16.1	0.6
E	20.7	1.0	11.3	21.1	1.7	9.8	0.4
F	18.5	0.9	9.8	19.3	1.6	12.3	0.8
G	16.9	0.6	9.3	17.6	0.9	8.7	0.7
H	15.9	0.4	69.7	16.9	0.6	94.1	0.9
I	15.4	0.4	17.7	16.6	0.4	34.3	1.2
J	14.7	0.6	15.4	16.4	0.4	60.1	1.7
WRR moraine ages				15.8	0.2[a]		
WRR Retreat				15.8	0.1		
LBA isolation age				15.8	0.1		
GB limiting age				15.6	0.1		

[a] Pooled standard deviation.

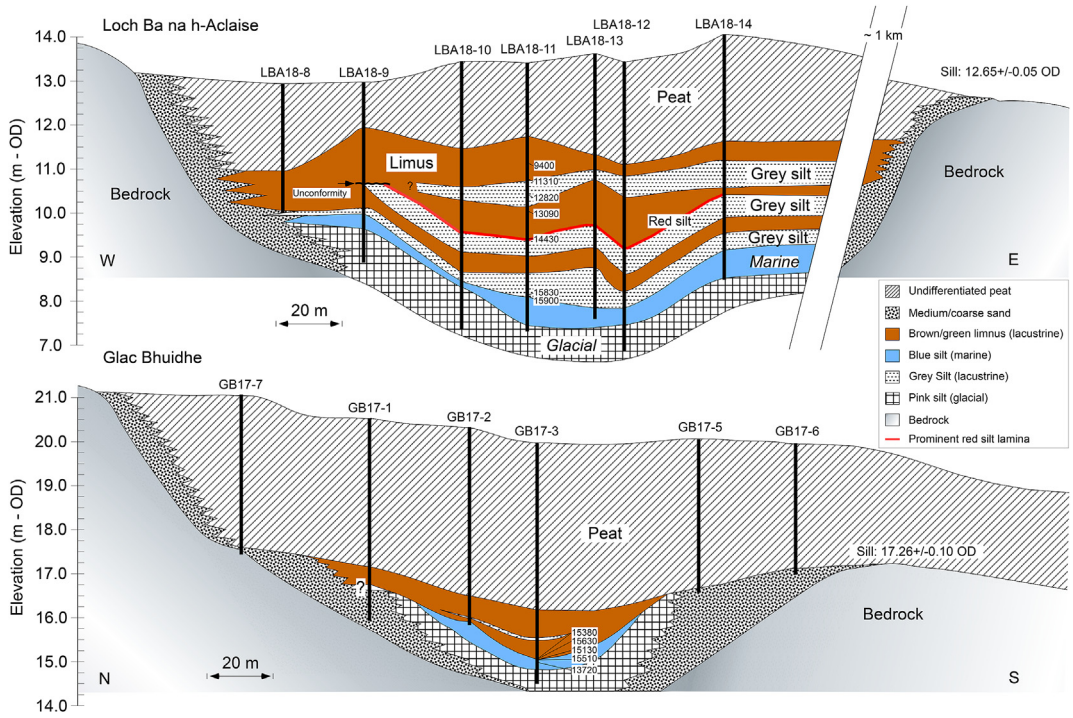

Fig. 3. Schematic figure showing the general stratigraphy found within northwestern Scotland isolation basins. For cores and stratigraphy from the isolation basins cored for this study see Supplementary Figs. S3 and S4.

536 cm to 9.40 cal ka BP (9.49–9.31 cal ka BP) at a depth of 233 cm (Table 1).

The radiocarbon ages from Glac Bhuidhe are not in stratigraphic order and suggest the isolation of Glac Bhuidhe occurred later than the lower-elevation Loch Bad na h-Achlaise (Table 1, Fig. 5). However, the ages from LBA18-11 are all in stratigraphic order while those from GB17-3 are not. Based on their out-of sequence and younger than anticipated ages, we interpret the material dated from GB17-3 to have been reworked, possibly as a result of the shallow water depth behind the sill, no more than ~2m (Fig. 5), at the time of isolation, and facilitated by the steep slopes surrounding the small basin. Therefore, the ages from Glac Bhuidhe are regarded as minimum ages for isolation and terrestrial limiting constraints on RSL. The two radiocarbon ages obtained from core IAN19-07 from Glac a' Chaochain at depths of 514 cm and 530 cm date to 13.96 cal ka BP (14.11–13.81 cal ka BP) and 15.21 cal ka BP (15.33–15.08 cal ka BP), respectively (Table 1, Fig. S6).

4.2.2. Recalibrated and RSL-extrapolated ages

The recalibrated radiocarbon ages were largely unchanged from previous calibrations. The recalibrated TCN ages of Bradwell et al. (2019) were older than the previous age estimates by 500–1000 years, but still within error of those originally calibrated by Bradwell et al. (2019) (Table S2). This difference is largely due to using the local Scottish scaling and production rates rather than an average of multiple models. Extrapolation of the RSL changes using the GIA model of Kuchar et al. (2012) at Fearnbeg and Gairloch suggest that the marine limits within the region date to 15.7–16.0 ka for the Applecross Peninsula and 16.1–16.5 ka for the Gairloch Peninsula. The B2011 and BC2020 models were not used in this analysis as they did not predict RSLs as high as the two observed marine limits corrected for the RSL indicative meaning (19.5 and 27.2 m for Gairloch and Applecross, respectively) during a time of ice-free conditions.

4.2.3. OxCal modeling

Our new OxCal model suggests generally older ages for the deglaciation of the MnIS compared to the original age model of Bradwell et al. (2019); although ages for sites A-G are within error (Table 2; S7). The age difference is greater for sites H-J and increases to the south (Table 2). The increasing difference with younger ages is driven largely by the addition of our new ages within Wester Ross. However, the pattern of MnIS retreat is generally unchanged, although we do find that the period of rapid retreat commenced about 700 years earlier at 17.6 ± 0.9 ka (versus 16.9 ± 0.6 ka) and at a rate ~35% faster within the inner MnIS (Table 2).

5. Discussion

5.1. Age of the Wester Ross Readvance

Suggested ages for the WRR have ranged from as old as 16.1 ka (Everest et al., 2006) to as young as 13.5 ka (Ballantyne et al., 2009). This range has made it difficult to correlate the WRR moraines with other deglacial moraines across the British Isles as well as regional and global climate proxies. Our new data favor older ages for the WRR. The oldest radiocarbon ages from both basins are 15.9 ± 0.2 cal ka BP (Loch Bad na h-Achlaise) and 15.5 ± 0.2 cal ka BP (Glac Bhuidhe), 500–1600 years older than the range reported by Ballantyne and Stone (2012) but within the range of individual ages reported for the nearest moraine – the Redpoint Moraine, with dates of 14.99 ± 0.75 ka to 15.93 ± 0.79 ka (Ballantyne and Stone, 2012). The WRR postdates 16.9 ± 0.6 ka when the MnIS retreated south of Wester Ross (location H; Fig. 1). Oxcal modelling

Fig. 4. Photographs of core LBA18-11 taken in the field overlain by the ages obtained from the core. See Table 1 for details on the radiocarbon ages including their errors.

incorporating the WRR TCN ages and our new radiocarbon constraints from the isolation basins indicate the area became ice free 15.8 ± 0.1 ka (Table 2). One issue with radiocarbon ages is the possibility of erroneously old ages due to contamination from old organic carbon (often released during deglaciation) as well as hardwater effects within the isolated waters (e.g. Turney et al., 2000). Although we cannot rule out such effects within Loch Bad na h-Achlaise, we tried to avoid the most common source of such hardwater effects (e.g. aquatic algae, fine organic detritus, etc.) by dating only macro- and micro-plant fragments and not the bulk sediment, which tends to be the source of much larger reservoir offsets (Turney et al., 2000). Although our analyses push back the Ballantyne and Stone (2012) timing of the WRR by 500 years, it is important to note that all the modelled probability distribution functions are still well within the relatively large error bars of the recalibrated TCN ages (Fig. 6).

Records of Northern Hemisphere climate recorded within the Greenland ice cores as well as ice-rafted debris records from the region (e.g. Stuiver and Grootes, 2000; Knutz et al., 2007) show centennial-scale variability in both the climate and ice sheet responses between 15 and 20 ka. The WRR may represent the ice-sheet response to one of these climatic oscillations, although local ice-sheet dynamics cannot be discounted. One such climatic oscillation is that associated with Heinrich Event H-1 (16–17.5 ka) as suggested by Everest et al. (2006) with evidence for advance during this time in other locations across the British Isles and Europe (e.g. McCabe et al., 1998; Knies et al., 2007; Ivy-Ochs et al., 2006). Alternatively, the WRR moraines could simply record the relaxation of the former tributary glaciers to the disappearance of the MnIS. More work is needed to determine the spatial extent of the WRR and whether it correlates with other similar-aged readvances across the former margins of the BIIS or regional climate events.

5.2. Relative sea-level changes

5.2.1. GIA predictions versus RSL observations

A comparison of the GIA model predictions with RSL observations and the timing of ice-free conditions at Fearnbeg, Gairloch, and Assynt reveals that in general the Kuchar et al. (2012) model works best for the Minch region (Fig. 7). For Fearnbeg and Assynt, the observations lie directly ontop of the Kuchar et al. (2012) GIA predictions, while for our new data at Gairloch, the observations lie between the Kuchar et al. (2012) GIA predictions and the other two GIA predictions. The other two models either predict RSLs that are too low or RSLs that are at the correct elevations but occur when the region is still covered in ice (Fig. 7). One criticism of the Kuchar et al. (2012) model has been over prediction of RSLs in other parts of Scotland (e.g. Shennan et al., 2018). Testing the maximum highstand elevations for the Minch around 19–20 ka remains difficult as the region was covered in ice at the time. However, for more peripheral regions of the ice sheet that deglaciated earlier (e.g. the Outer Hebrides, North Rona, etc.), no elevated shorelines at the elevations predicted by the Kuchar et al. (2012) model (80–100+ m) have been described (e.g. Shennan et al., 2018). The highest marine features described on North Lewis and North Rona are less than ~20 m in elevation (Baden-Powell, 1938; Stewart, 1932); although, neither have been dated and are usually attributed to earlier interglacials (Smith et al., 2019). Thus, for the outer shelf through the Outer Hebrides, predictions using the other two GIA models may be more representative of the RSL history experienced during the early retreat of the MnIS. These regional variations in the preferred model highlight the need for more RSL data and continued refinement of the ice-sheet and GIA models for the BIIS.

5.2.2. RSL controls on ice retreat

Although a landward dipping slope, the potential loss of an ice shelf "buttressing" the ice stream, and bed strength were likely important controls on back stepping of the MnIS (Bradwell et al., 2019; Gandy et al., 2018), the large increase in the rate of MnIS retreat between 17.6 and 16.4 ka corresponds to the region where the ice front switched from experiencing RSL fall to RSL rise (Figs. 8 and 9). RSL was also rising during the earliest stages of MnIS retreat (e.g. prior to location E; Fig. 8; Fig. 9 inset), but GIA model predictions diverge greatly at these times and no RSL data are available to test these predictions. In addition, Earth was experiencing a full glacial climate regime at that time. Furthermore, rates of RSL rise experienced during this time from 17.6 ka to 16.4 ka were 5.5 mm/yr, 21.4 mm/yr, and 24.6 mm/yr for the Kuchar, B2011, and BC2020 models, respectively, with a total amount of RSL rise experienced over the ~1200-year time period of 6.6 m, 25.6 m, and 29.5 m, respectively. Thus, RSL rise cannot be excluded as a potential driver of the rapid retreat of the MnIS and may have contributed to its rapid retreat. This behavior highlights the role that RSL could play in driving marine ice sheet instability and retreat.

5.3. Implications regarding marine ice sheet instability

Marine ice sheet instability is thought to be dampened by negative feedbacks related to post-glacial rebound as an ice sheet retreats (Gomez et al., 2010). In this model scenario, the magnitude

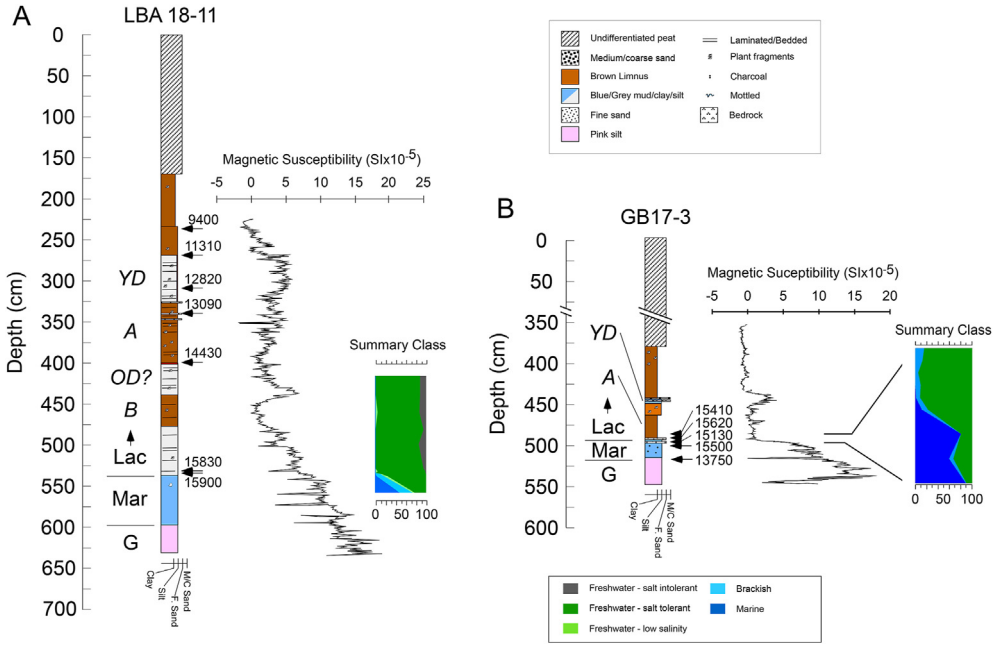

Fig. 5. Core description, magnetic susceptibility, and diatom summary for cores LBA18-11 (A) and GB17-13 (B). Numbers next to each core description indicate median radiocarbon ages (See Table 1 for radiocarbon error ranges) while letters left of the column represent interpreted depositional environments (G = Glacial, Mar = Marine, Lac = Lacustrine) and climate phase in italics (B = Bølling Warm Period, OD? = potential Older Dryas, A = Allerod Warm Period, and YD = Younger Dryas). Within the diatom summary, green represent freshwater species while blues represent marine/brackish species. For full diatom counts see Fig. S5. (For interpretation of the references to color in this figure legend, the reader is referred to the Web version of this article.)

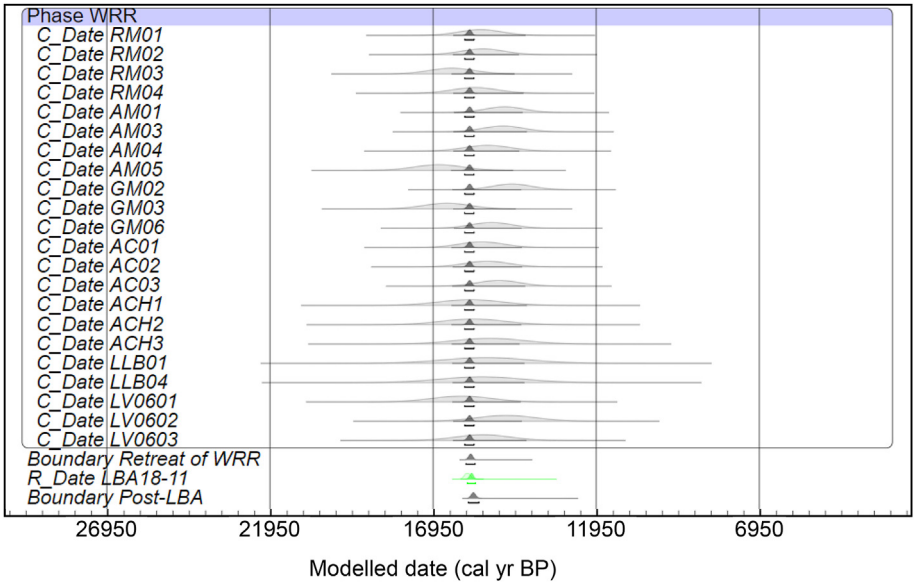

Fig. 6. Probability distribution functions of the recalibrated WRR TCN ages as well as our new age from Loch Bad na h-Achlaise as produced by our OxCal model (see Fig. S7 for the full model output).

of rebound due to GIA is significant enough to overcome the fore-deepening the ice sheet encounters as it retreats (Gomez et al., 2010), thus stabilizing the marine ice stream. Such a process does not appear to have operated to slow the retreat of the MnIS (Fig. 8). One possibility for not seeing a response is that the water depths in which the MnIS was retreating into were too great for the rebound to overcome. (We note that the water depths within the Minch (<300 m; Fig. 2) are similar to those beneath many of the ice streams in Antarctica as well as Greenland – i.e. Patton et al., 2016). However, our RSL predictions suggest it is not simply a matter of too little rebound, but of RSL rise rather than rebound (e.g. Fig. 8). Why was the retreat of the MnIS not accompanied by post-glacial rebound? First, the local ice margins and Earth rheology beneath the MnIS may have played a role in hindering post-glacial rebound. Numerical models predicting the stabilizing effect of post-glacial rebound generally consider a radially symmetric ice sheet (Gomez et al., 2010) or a weak Earth rheology (Kachuck et al., 2020), neither of which apply to the MnIS. For the MnIS, its retreat was

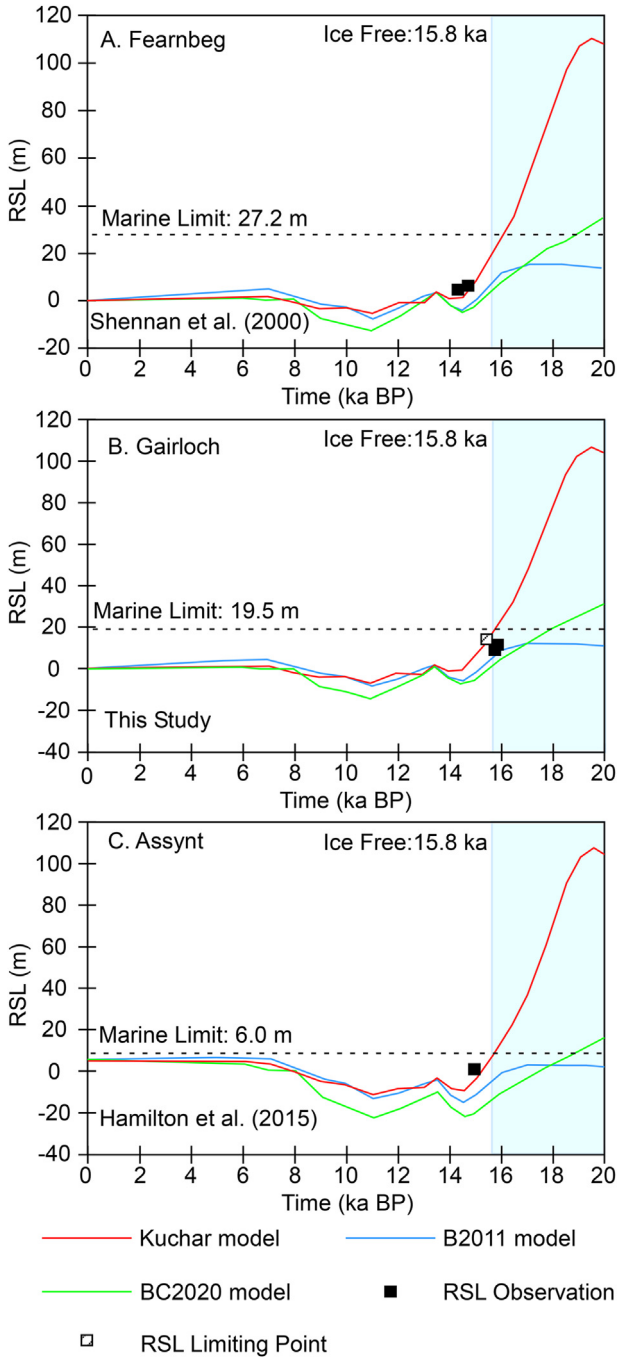

Fig. 7. Comparison of RSL observations to three GIA model predictions for A.) Fearnbeg, B.) Gairloch (including both Loch Bad na h-Achlaise and Glac Bhudhe), and C.) Assynt. See Fig. 1 for geographic locations. RSL observations for A and C are from (Shennan et al., 2000) and Hamilton et al. (2015), respectively, while those for B are from this study. The marine limits for A are from Sissons (1977) and Dawson (2009), while those from B are from Sissons and Dawson (1981) and those from C are from Shennan et al. (2000) and Hamilton et al. (2015).

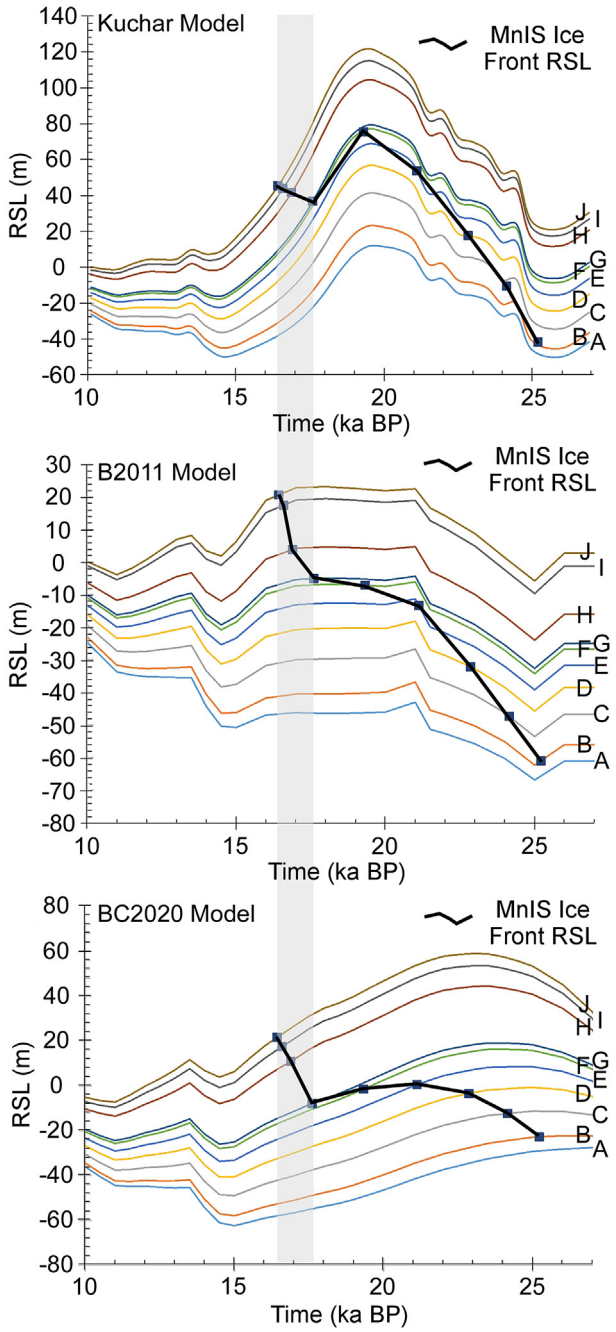

Fig. 8. Glacial isostatic adjustment model predictions of RSL experienced at the MnIS ice front through time using the models of A.) Kuchar et al. (2012), B.) B2011, Bradley et al. (2011), and C.) BC 2020, Clark et al. (2017). Letters represent the ice front locations shown in Fig. 1. The grey box outlines the timing of the rapid retreat of the MnIS from 17.6-16.4 ka.

along an indented part of the BIIS with significant remnant ice masses remaining to the east, west, and south (Bradwell et al., 2008a; b, 2021; Ballantyne and Small, 2018). These larger remaining ice masses are the more dominant control over the regional rebound signal such that it may have overprinted/counteracted the local rebound signal from the MnIS retreat.

Second, unlike the weak Earth rheology present under portions of West Antarctica (e.g. Simms et al., 2018; Barletta et al., 2018) to which models such as Gomez et al. (2010) and Kachuck et al. (2020) are parameterized, Scotland is underlain by an "average" Earth structure (Lambeck and Purcell, 2001; Bradley et al., 2011) and thus is less likely to be responsive to smaller ice load changes. For example, recent GIA models for West Antarctica utilize upper mantle viscosities of ~10^{18} Pa s (Simms et al., 2012; Nield et al., 2014; Kachuck et al., 2020; Wan et al., 2021) while most for Scotland use upper-mantle viscosities of ~10^{20}–10^{21} Pa s (Lambeck et al., 1996; Bradley et al., 2011). Furthermore, the width of the

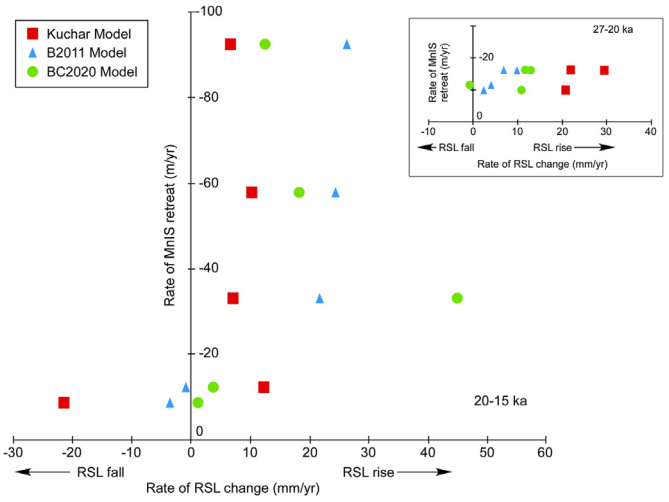

Fig. 9. Comparison between rates of RSL rise and retreat of the MnIS ice front for the time period from 20-15 ka. Inset is the same but for the time period from 27-20 ka.

load (~50 km within the inner Minch) is on the same order as the lithospheric thickness beneath Scotland (e.g. 71 km for the model of Bradley et al., 2011). Thus, the geologic setting of the ice stream must be taken into account when considering the stabilizing impact of post-glacial rebound. A third factor that may have contributed to instability of the MnIS is the speed of retreat. In a model stability analysis, Kachuck et al. (2020) point out that if the ice stream retreats faster than the Earth can respond, such a stabilizing influence will not be felt. That may have been the case for the MnIS.

If the stabilizing impact of post-glacial rebound is dependent on setting, it has important implications for the ongoing retreat of ice streams in polar regions. Unlike West Antarctic, but similar to the MnIS, the ice streams of Greenland (e.g. Wake et al., 2016) and the marine-based portions of East Antarctica such as the Wilkes subglacial basin (Mengel and Levermann, 2014) are not underlain by a weak rheology and thus may be less influenced by the stabilizing effect of post-glacial rebound during their retreat. Although the stabilizing mechanism of post-glacial rebound provides some grounds for optimism regarding the fate of West Antarctica, the same may not be true for much of Greenland and East Antarctica.

6. Conclusions

We provide new constraints on the sea-level and deglacial history of western Scotland. Our new RSL record suggests that RSL fell along the eastern Minch by more than 14.2 ± 0.4 m since deglaciation reaching 11.4 ± 0.4 m as early as 15.9 ± 0.2 cal ka BP. Our new ages also further refine the age of the Wester Ross Readvance, suggesting it culminated around 15.8 ± 0.1 ka, 500 years earlier than some suggestions. The WRR may represent a response of the Scottish glaciers to Heinrich Event 1 or simply a de-buttressing of the mainland Scottish glaciers following the retreat of the Minch Ice Stream. Our new RSL constraints fit better with GIA models with thicker ice over western Scotland. However, such models overestimate the magnitude of RSL fall for other regions of Scotland highlighting the need for continued refinement of ice-sheet and GIA models for the region.

In conjunction with three different GIA models we use our new RSL data to reconstruct the RSL changes experienced by the Minch Ice Stream during its retreat. We find that a previously documented period of accelerated ice stream retreat not only corresponds to a landward deepening slope and change in trough substrate but also the region in which RSL changes from RSL fall to RSL rise, suggesting RSL rise may have played a joint role in driving the rapid retreat of the MnIS at ~17.6 ka. Unlike some conceptual models, we find that post-glacial rebound did not provide a stabilizing mechanism during the retreat of the MnIS. The absence of this feedback mechanism to develop was likely due to the relatively strong rheology beneath Scotland and the indented ice front that marked the NW margin of the ice sheet over Scotland during retreat of the MnIS. This finding highlights the need to consider the local conditions of the ice stream and its setting on the ability of post-glacial rebound to stop runaway ice sheet retreat.

Author contributions

ARS, LB, and IS designed the experiment. ARS, LB, IS, EB, AL, and JS conducted fieldwork. ARS and DO conducting the radiocarbon age analysis. DS recalibrated the TCN ages. SLB conducted the GIA calculations. ARS and DS conducted the OxCal modeling. ARS wrote the manuscript with input from LB, IS, SB, DS, and the rest of the authors.

Declaration of competing interest

The authors declare that they have no known competing financial interests or personal relationships that could have appeared to influence the work reported in this paper.

Acknowledgements

This research was largely conducted while ARS was on sabbatical at Durham University, which was made possible through support from the US-UK Fulbright Commission and Durham University. Additional financial support came through a UCSB Academic Faculty Senate Grant and the Durham University Geography Department. DS is supported by a NERC Independent Research Fellowship NE/T011963/1. Cameron Gernant and Sara Nethercutt are thanked for their help in the field as is John Southon at UCI for help in radiocarbon dating. We also wish to thank Lorraine Lisiecki for comments on the manuscript and discussion.

Appendix A. Supplementary data

Supplementary data to this article can be found online at https://doi.org/10.1016/j.quascirev.2021.107366.

References

Baden-Powell, D.F.W., 1938. On the glacial and interglacial marine beds of Northern Lewis. Geol. Mag. 75, 395–409.
Balco, G., Stone, J.O., Lifton, N.A., Dunai, T.J., 2008. A complete and easily accessible means of calculating surface exposure ages or erosion rates from ^{10}Be and ^{26}Al measurements. Quat. Geochronol. 3, 174–195.
Ballantyne, C.K., Schnabel, C., Xu, S., 2009. Readvance of the last British-Irish ice sheet during Greenland interstade 1 (GI-1): the wester Ross readvance, NW Scotland. Quat. Sci. Rev. 28, 783–789.
Ballantyne, C.K., Small, D., 2018. The last Scottish ice sheet. Earth Environ. Sci. Trans. Royal Soc. Edinburgh 110, 93–131.
Ballantyne, C.K., Stone, J.O., 2012. Did large ice caps persist on low ground in northwest Scotland during the Lateglacial Interstade? J. Quat. Sci. 27, 297–306.
Barletta, V.R., Bevis, M., Smith, B.E., Wilson, T., Brown, A., Bordoni, A., Willis, M., Khan, S.A., Rovira-Navarro, M., Dalziel, I., Smalley, R.J., Kendrick, E., Konfal, S., Caccamise, D.J.I., Aster, R.C., Nyblade, A., Wiens, D.A., 2018. Observed rapid bedrock uplift in Amundsen Sea Embayment promotes ice-sheet stability. Science 360.
Best, L., Simms, A.R., Brader, M., Lloyd, J., Sefton, J., Shennan, I., (in press). Local and regional constraints on Relative sea-level changes in southern Isle of Skye,

Scotland, since the last glacial maximum. J. Quat. Sci. doi.org/10.1002/jqs.3376.
Bart, P.J., Tulaczyk, S., 2020. A significant acceleration of ice volume discharge preceded a major retreat of a West Antarctic paleo-ice stream. Geology 48, 313–317.
Bradley, S.L., Milne, G.A., Shennan, I., Edwards, R., 2011. An improved glacial isostatic adjustment model for the British Isles. J. Quat. Sci. 26, 541–552.
Bradwell, T., Fabel, D., Clark, C.D., Chiverrell, R.C., Small, D., Smedley, R.K., Saher, M.H., Moreton, S.G., Dove, D., Callard, S.L., Duller, G.A.T., Medialdea, A., Bateman, M.D., Burke, M.J., McDonald, N., Gilgannon, S., Morgan, S., Roberts, D.H., O'Cofaigh, C., 2021. Pattern, style and timing of British-Irish Ice Sheet advance and retreat over the last 45 000 years: evidence from NW Scotland and the adjacent continental shelf. J. Quat. Sci. 36, 871–933.
Bradwell, T., Fabel, D., Stoker, M., Mathers, H., McHargue, L., Howe, J., 2008a. Ice caps existed throughout the lateglacial interstadial in northern Scotland. J. Quat. Sci. 23, 401–407.
Bradwell, T., Small, D., Fabel, D., Smedley, R.K., Clark, C.D., Saher, M.H., Callard, S.L., Chiverrell, R.C., Dove, D., Moreton, S.G., Roberts, D.H., Duller, G.A.T., O' Cofaigh, C., 2019. Ice-stream demise dynamically conditioned by trough shape and bed strength. Sci. Adv. 5, eaau1380.
Bradwell, T., Stoker, M.S., 2015. Submarine sediment and landform record of a palaeo-ice stream within the British-Irish Ice Sheet. Boreas 44, 255–276.
Bradwell, T., Stoker, M.S., Golledge, N.R., Wilson, C.K., Merritt, J.W., Long, D., Everest, J.D., Hestvik, O.B., Stevenson, A.G., Hubbard, A.L., Finlayson, A.G., Mathers, H.E., 2008b. The northern sector of the last British Ice Sheet: maximum extent and demise. Earth Sci. Rev. 88, 207–226.
Bronk Ramsey, C., 2009. Bayesian analysis of radiocarbon dates. Radiocarbon 51, 337–360.
Bronk Ramsey, C., Albert, P.G., Blockley, S.P.E., Hardiman, M., Housley, R.A., Lane, C.S., Lee, S., Matthews, I.P., Smith, V.C., Lowe, J.J., 2015. Improved estimates for key late Quaternary European tephra horizons in the RESET lattice. Quat. Sci. Rev. 118, 18–32.
Brooks, S.J., Matthews, I.P., Birks, H.H., Birks, H.J.B., 2012. High resolution Lateglacial and early-Holocene summer air temperature records from Scotland inferred from chironomid assemblages. Quat. Sci. Rev. 41, 67–82.
Clark, C.D., Ely, J.C., Greenwood, S.L., Hughes, A.L.C., Meehan, R., Barr, I.D., Bateman, M.D., Bradwell, T., Doole, J., Evans, D.J.A., Jordan, C.J., Monteys, X., Pellicer, X.M., Sheehy, M., 2017. BRITICE Glacial Map, version 2: a map and GIS database of glacial landforms of the last British-Irish Ice Sheet. Boreas 47, 11–27.
Davies, B.J., Livingstone, S.J., Roberts, D.H., Evans, D.J.A., Gheorghiu, D.M., Cofaigh, OC., 2019. Dynamic ice stream retreat in the central sector of the last British-Irish Ice Sheet. Quat. Sci. Rev. 225, 105989.
Dawson, A., 2009. 7.1 Late glacial and Holocene relative sea-level change in Applecross, Raasay and eastern Skye. In: Hardy, K., Wickham-Jones, C. (Eds.), Scotland's First Settlers. The Society of Antiquaries of Scotland.
Dowdeswell, J.A., Ottensen, D., Evans, J., O Cofaigh, C., Anderson, J.B., 2008. Submarine glacial landforms and rates of ice-stream collapse. Geology 36, 819–822.
Everest, J.D., Bradwell, T., Fogwell, C.J., Kubik, P.W., 2006. Cosmogenic 10Be age constraints for the wester Ross readvance moraine: insights into British ice-sheet behavior. Geogr. Ann. Phys. Geogr. 88, 9–17.
Fabel, D., Ballantyne, C.K., Xu, S., 2012. Trimlines, blockfields, mountain-top erratics and the vertical dimensions of the last British-Irish Ice Sheet in NW Scotland. Quat. Sci. Rev. 55, 91–102.
Gandy, N., Gregoire, L.J., Ely, J.C., Clark, C.D., Hodgson, D.M., Lee, V., Bradwell, T., Ivanovic, R.F., 2018. Marine ice sheet instability and ice shelf buttressing of the Minch Ice Stream, northwest Scotland. Cryosphere 12, 3635–3651.
Gomez, N., Mitrovica, J.X., Huybers, P., Clark, P.U., 2010. Sea level as a stabilizing factor for marine-ice-sheet grounding lines. Nat. Geosci. 3, 850–853.
Gowan, E.J., Tregoning, P., Purcell, A., Lea, J., Fransner, O.J., Noormets, R., Dowdeswell, J.A., 2016. ICESHEET 1.0: a program to produce paleo-ice sheet reconstructions with minimal assumptions. Geosci. Model Dev. (GMD) 9, 1673–1682.
Greenwood, S.L., Simkins, L.M., Winsborrow, M.C.M., Bjarnadottir, L.R., 2021. Exceptions to bed-controlled ice sheet flow and retreat from glaciated continental margins worldwide. Sci. Adv. 7, eabb6291.
Hamilton, C.A., Lloyd, J.M., Barlow, N.L.M., Innes, J.B., Flecker, R., Thomas, C.P., 2015. Late glacial to Holocene relative sea-level change in Assynt, northwest Scotland, UK. Quat. Res. 84, 214–222.
Hubbard, A., Bradwell, T., Golledge, N., Hall, A., Patton, H., Sugden, D., Cooper, R., Stoker, M., 2009. Dynamic cycles, ice streams and their impact on the extent, chronology, and deglaciation of the British-Irish ice sheet. Quat. Sci. Rev. 28, 759–777.
Hughes, A.L.C., Gyllencreutz, R., Lohne, O.S., Mangerud, J., Svendsen, J.I., 2016. The last Eurasian ice sheets - a chronological database and time-slice reconstruction, DATED-1. Boreas 45, 1–45.
Ivy-Ochs, S., Kerschner, H., Kubik, P.W., Schlüchter, C., 2006. Glacier response in the European alps to Heinrich event 1 cooling: the Gschnitz stadial. J. Quat. Sci. 21, 115–130.
Kachuck, S.B., Martin, D.F., Bassis, J.N., Price, S.F., 2020. Rapid viscoelastic deformation slows marine ice sheet instability at Pine Island Glacier. Geophys. Res. Lett. 47, e2019GL086446.
Knies, J., Vogt, C., Matthiessen, J., Nam, S.-I., Ottesen, D., Rise, L., Bargel, T., Eilertsen, R.S., 2007. Re-advance of the Fennoscandian ice sheet during Heinrich event 1. Mar. Geol. 240, 1–18.
Knutz, P.C., Zahn, R., Hall, I.R., 2007. Centennial-scale variability of the British Ice Sheet: implications for climate forcing and Atlantic meridional overturning circulation during the last deglaciation. Paleoceanography 22, PA1207.
Kuchar, J., Milne, G., Hubbard, A., Patton, H., Bradley, S., Shennan, I., Edwards, R., 2012. Evaluation of a numerical model of the British-Irish ice sheet using relative sea-level data: implications for the interpretation of trimline observations. J. Quat. Sci. 27, 597–605.
Lambeck, K., Johnston, P., Smither, C., Nakada, M., 1996. Glacial rebound of the British Isles – III. Constraints on mantle viscosity. Geophys. J. Int. 125, 340–354.
Lambeck, K., Purcell, A.P., 2001. sea-level change in the Irish sea since the last glacial maximum: constraints from isostatic modelling. J. Quat. Sci. 16, 497–506.
Lifton, N., Sato, T., Dunai, T.J., 2014. Scaling in situ cosmogenic nuclide production rates using analytical approximations to atmospheric cosmic-ray fluxes. Earth Planet Sci. Lett. 386, 149–160.
MacLeod, A., Palmer, A., Lowe, J., Rose, J., Bryant, C., Merritt, J., 2011. Timing of glacier response to Younger Dryas climatic cooling in Scotland. Global Planet. Change 79, 264–274.
McCabe, M., Knight, J., McCarron, S., 1998. Evidence for Heinrich event 1 in the British Isles. J. Quat. Sci. 13, 549–568.
Mengel, M., Levermann, A., 2014. Ice plug prevents irreversible discharge from East Antarctica. Nat. Clim. Change 4, 451–455.
Mercer, J.H., 1978. West Antarctica ice sheet and CO2 greenhouse effect: a threat of disaster. Nature 271, 321–325.
Nield, G.A., Barletta, V.R., Bordoni, A., King, M.A., Whitehouse, P.L., Clarke, P.J., Domack, E., Scambos, T.A., Berthier, E., 2014. Rapid bedrock uplift in the Antarctic Peninsula explained by viscoelastic response to recent ice unloading. Earth Planet Sci. Lett. 397, 32–41.
Palmer, A.P., Matthews, I.P., Lowe, J.J., MacLeod, A., Grant, R., 2020. A revised chronology for the growth and demise of Loch Lomond Readvance ('Younger Dryas') ice lobes in the Lochaber area, Scotland. Quat. Sci. Rev. 248, 106548.
Patton, H., Swift, D.A., Clark, C.D., Livingstone, S.J., Cook, S.J., 2016. Distribution and characteristics of overdeepenings beneath the Greenland and Antarctic ice sheets: implications for overdeepening origin and evolution. Quat. Sci. Rev. 148, 128–145.
Reimer, P.J., Austin, W.E.N., Bard, E., Bayliss, A., Blackwell, P.G., Bronk Ramsey, C., Butzin, M., Cheng, H., Edwards, R.L., Friedrich, M., Grootes, P.M., Guilderson, T.P., Hajdas, I., Heaton, T.J., Hogg, A.G., Hughen, K.A., Kromer, B., Manning, S.W., Muscheler, R., Palmer, J.G., Pearson, C., Van der Plicht, J., Reimer, R.W., Richards, D.A., Scott, E.M., Southon, J.R., Turney, C.S.M., Wacker, L., Adolphi, F., Buntgen, U., Capano, M., Fahrni, S.M., Fogmann-Schultz, A., Friedrich, R., Kohler, P., Kudsk, S., Miyake, F., Olsen, J., Reinig, F., Sakamoto, M., Sookdeo, A., Talamo, S., 2020. The IntCal20 Northern Hemisphere radiocarbon age calibration curve (0-55 cal kBP). Radiocarbon 62, 725–757.
Robinson, M., Ballantyne, C.K., 1979. Evidence for a glacial readvance pre-dating the Loch Lomond advance in wester Ross. Scot. J. Geol. 15, 271–277.
Scourse, J., Saher, M., Van Landeghem, K.J.J., Lockhart, E., Purcell, C., Callard, L., Roseby, Z., Allinson, B., Pienkowski, A.J., O'Cofaigh, C., Praeg, D., Ward, S., Chiverrell, R., Moreton, S., Fabel, D., Clark, C.D., 2019. Advance and retreat of the marine-terminating Irish sea ice stream into the Celtic sea during the last glacial: timing and maximum extent. Mar. Geol. 412, 53–68.
Selby, K.A., Smith, D.E., 2007. Late Devensian and Holocene Relative sea-level changes on the Isle of Skye, Scotland, UK. J. Quat. Sci. 22, 119–139.
Shennan, I., Bradley, S.L., Edwards, R., 2018. relative sea-level changes and crustal movements in Britain and Ireland since the last glacial maximum. Quat. Sci. Rev. 188, 143–159.
Shennan, I., Lambeck, K., Horton, B., Innes, J., Kennington, K., Lloyd, J., Rutherford, M.M., 2000. Late Devensian and Holocene records of relative sea-level changes in northwest Scotland and their implications for glacio-hydro-isostatic modelling. Quat. Sci. Rev. 19, 1103–1135.
Simms, A.R., Ivins, E.R., DeWitt, R., Kouremenos, P., Simkins, L.M., 2012. Timing of the most recent Neoglacial advance and retreat in the south Shetland islands, antarctic Peninsula: insights from raised beaches and Holocene uplift rates. Quat. Sci. Rev. 47, 41–55.
Simms, A.R., Whitehouse, P.L., Simkins, L.M., Nield, G., DeWitt, R., Bentley, M., 2018. Late Holocene relative sea levels near Palmer Station, northern Antarctic Peninsula, strongly controlled by late Holocene ice-mass changes. Quat. Sci. Rev. 199, 49–59.
Sissons, J.B., 1977. The Loch Lomond readvance in the northern mainland of Scotland. In: Gray, J.M., Lowe, J.J. (Eds.), Studies in the Scottish Lateglacial Environment. Pergamon, Oxford, pp. 45–59.
Sissons, J.B., Dawson, A.G., 1981. Former sea-levels and ice limits in part of Wester Ross, northwest Scotland. Proc. Geologists' Assoc. 92, 115–124.
Small, D., Fabel, D., 2016. Was Scotland deglaciated during the younger Dryas? Quat. Sci. Rev. 145, 259–263.
Small, D., Smedley, R.K., Chiverrell, R.C., Scourse, J.D., O'Cofaigh, C., Duller, G.A.T., McCarron, S., Burke, M.J., Evans, D.J.A., Fabel, D., Gheorghiu, D.M., Thomas, G.S.P., Xu, S., Clark, C.D., 2018. Trough geometry was a greater influence than climate-ocean forcing in regulating retreat of the marine-based Irish-Sea Ice Stream. Geol. Soc. Am. Bull. 130, 1981–1999.
Smith, D.E., Barlow, N.L.M., Bradley, S.L., Firth, C.R., Hall, A.M., Jordon, J.T., Long, D., 2019. Quaternary sea level change in Scotland. Earth Environ. Sci. Trans. Royal Soc. Edinburgh 110, 219–256.
Stewart, M., 1932. Notes on the geology of north Rona. Geol. Mag. 69, 179–185.
Stoker, M.S., Bradwell, T., Howe, J.A., Wilkinson, I.P., McIntyre, K., 2009. Lateglacial ice-cap dynamics in NW Scotland: evidence from the fjords of the Summer Isles region. Quat. Sci. Rev. 28, 3161–3184.

Stuiver, M., Grootes, P.M., 2000. GISP2 oxygen isotope ratios. Quat. Res. 53, 277–284.
Turney, C.S.M., Coope, G.R., Harkness, D.D., Lowe, J.J., Walker, M.J.C., 2000. Implications for the dating of Wisconsinan (Weichselian) Late-Glacial events of systematic radiocarbon age differences between terrestrial plant macrofossils from a site in SW Ireland. Quat. Res. 53, 114–121.
Wan, J.X.W., Gomez, N., Latychev, K., Han, H.K., 2021. Resolving GIA in response to modern and future ice loss at marine grounding lines in West Antarctica. Cryosphere Discuss. 1–32. https://doi.org/10.5194/tc-2021-232.
Wake, L.M., Lecavalier, B.S., Bevis, M., 2016. Glacial isostatic adjustment (GIA) in Greenland: a review. Curr. Clim. Change Rep. 2, 101–111.
Weertman, J., 1974. Stability of the junction of an ice sheet and an ice shelf. J. Glaciol. 13, 3–11.